Chaos
An Interdisciplinary Journal of Nonlinear Science

RESEARCH ARTICLE | FEBRUARY 21 2023

Stochastic and deterministic dynamics in networks with excitable nodes

M. Rahimi-Majd; J. G. Restrepo ; M. N. Najafi

Chaos 33, 023134 (2023)
https://doi.org/10.1063/5.0103806

Stochastic and deterministic dynamics in networks with excitable nodes

Cite as: Chaos 33, 023134 (2023); doi: 10.1063/5.0103806
Submitted: 17 June 2022 · Accepted: 27 January 2023 ·
Published Online: 21 February 2023

M. Rahimi-Majd,[1] J. G. Restrepo,[2,a)] and M. N. Najafi[3,a)]

AFFILIATIONS

[1]Department of Physics, Shahid Beheshti University, 1983969411 Tehran, Iran
[2]Department of Applied Mathematics, University of Colorado, Boulder, Colorado 80309, USA
[3]Department of Physics, University of Mohaghegh Ardabili, 5619911367 Ardabil, Iran

[a)]**Authors to whom correspondence should be addressed:** juanga@colorado.edu and morteza.nattagh@gmail.com

ABSTRACT

Networks of excitable systems provide a flexible and tractable model for various phenomena in biology, social sciences, and physics. A large class of such models undergo a continuous phase transition as the excitability of the nodes is increased. However, models of excitability that result in this continuous phase transition are based implicitly on the assumption that the probability that a node gets excited, its transfer function, is linear for small inputs. In this paper, we consider the effect of cooperative excitations, and more generally the case of a nonlinear transfer function, on the collective dynamics of networks of excitable systems. We find that the introduction of any amount of nonlinearity changes qualitatively the dynamical properties of the system, inducing a discontinuous phase transition and hysteresis. We develop a mean-field theory that allows us to understand the features of the dynamics with a one-dimensional map. We also study theoretically and numerically finite-size effects by examining the fate of initial conditions where only one node is excited in large but finite networks. Our results show that nonlinear transfer functions result in a rich effective phase diagram for finite networks, and that one should be careful when interpreting predictions of models that assume noncooperative excitations.

Networks of coupled excitable systems undergo a phase transition as the excitability of the nodes is increased. Critical behavior at the tipping point of this phase transition has been associated to various properties observed in neuronal networks, such as optimized dynamic range and information processing.[1–8] Models of these systems usually assume that one excited node is enough to produce an excitation in another node. Here, we study the effect of cooperative excitations by considering a nonlinear transfer function that interpolates between linear, stochastic excitations, and a threshold-type deterministic excitation rule. We find that any amount of nonlinearity qualitatively changes the properties of the phase transition and produces a rich-phase diagram including bistability, hysteresis, and discontinuous transitions. We also study finite-size networks and find that, even for large network size, the effective phase diagram can be very different from the phase diagram predicted for infinite networks.

I. INTRODUCTION

The collective behavior of networks comprised of excitable nodes has found applications in many systems ranging from avalanches of neuronal bursting in the mammalian cortex[9,10] and neuroscience as a whole[3,4,11–14] to epidemiology[15,16] and social systems.[1,15] The dynamics of these systems can be very rich, including behaviors such as a second-order non-equilibrium phase transition separating the absorbing state from the super-critical state,[1–3] oscillatory behavior,[17,18] and a critical transition line with varying exponents.[19] One of the most important properties of systems with excitable dynamics is criticality, the state where the strength of interactions is balanced at the tipping point of a phase transition. It has been shown that operating in this regime might offer various functional advantages,[5–7,20] including optimal dynamic range,[1,2,4,8,21] synaptic learning,[14] optimal control,[5] and optimal information processing.[1] This state can be achieved in a self-organized

fashion[22] (as expected in the brain), which is a source of many theoretical studies based on network plasticity (brain plasticity in Ref. 13) and experimental studies, e.g., by tuning the ratios of excitation to inhibition for cortex slice cultures grown on planar microelectrode arrays.[4] The basic assumption in the theoretical studies is that when the excitation probability of a single node p_t is small, the master equations can be linearized.[2] However, this assumption is violated for systems with cooperative excitation rules and, more generally, for systems with transfer functions that have nonlinear leading order terms. An extreme example is that of deterministic dynamics with a threshold, which applies for sandpile-like dynamics on complex networks[23–25] or in social contagion models.[26] In this paper, we uncover a rich phase space by introducing and analyzing a model that interpolates between stochastic and deterministic dynamics. We find that any amount of nonlinearity qualitatively changes the properties of phase transition and produces a rich phase diagram including bistability, hysteresis, and discontinuous transitions. A mean-field analysis allows us to understand the collective dynamics of the system. In addition to studying the effect of a nonlinear transfer function, we explore the effect of a finite network. Theoretical analyses are usually carried out in the $N \to \infty$ limit, and initial conditions are chosen by implicitly assuming that a macroscopic fraction of nodes is initially excited. Here, we also consider the case where N is large but finite, and the system is started with only *one* excited node. We show that the effective phase diagram for this case is qualitatively different from the phase diagram obtained when a constant positive fraction of the $N \to \infty$ nodes is excited.

The structure of this paper is as follows. In Sec. II, we review previous results on the Kinouchi–Copelli model and non-cooperative excitations. In Sec. III, we present a model for excitable networks that interpolates between linear stochastic dynamics and deterministic dynamics. In Sec. IV, we study the dynamics of the generalized model numerically and analytically. In Sec. V, we consider the effective phase diagram of the model for finite-size networks, and in Sec. VI, we discuss our results.

II. BACKGROUND

In this section, we review previous results on the Kinouchi–Copelli model[1] and discuss how it can be generalized to account for cooperative excitation rules.

The Kinouchi–Copelli model consists of a network of N excitable nodes labeled $i = 1, \ldots, N$ that evolve in discrete time steps $t = 0, 1, \ldots$. A node i can be in the rest state [characterized by a variable $x_i(t) = 0$], excited [$x_i(t) = 1$], or in $m - 1$ refractory states [$x_i(t) = 2, 3, \ldots, m$]. If node i is in the rest state, it becomes excited in the next step by a neighboring excited node j with probability A_{ij} or independently by an external stimulus with probability η, where η represents an external stochastic stimulus. The nodes in the refractory state evolve as $x_i(t+1) = x_i(t) + 1$ if $1 \le x_i(t) < m - 1$ and $x_i(t+1) = 0$ if $x_i(t) = m$. It was shown by Larremore *et al.*[2] that the largest eigenvalue λ of the matrix A with entries A_{ij} and its associated eigenvector play a prominent role in determining the collective dynamics of the system. For $\lambda < \lambda_c \equiv 1$, the system falls into the absorbing state where no node is excited, while for $\lambda > \lambda_c$, the activity of the system saturates eventually to a state where a macroscopic fraction of the nodes are excited. The inclusion of a refractory period causes additionally another transition point ($\lambda_b \equiv 2$) at which the system undergoes bifurcation to an oscillatory regime.[17] Therefore, the phase diagram of these systems is given by

$$\begin{cases} 0 \le \lambda < \lambda_c & \text{subcritical regime,} \\ \lambda_c < \lambda < \lambda_b & \text{supercritical regime,} \\ \lambda > \lambda_b & \text{oscillatory regime.} \end{cases} \tag{1}$$

The key strategy in this work, which was followed later by many authors for other dynamical models,[3,17,21] was to linearize the governing master equations with respect to the nodes' firing probability being small near the transition point λ_c. This strategy relies on the probability of a node being excited in the next time step p_i^{t+1} to have leading-order *linear* terms in terms of probabilities that other nodes are excited at the current time, $\mathbf{p}^t$, which we call *linear stochasticity*. Many additional effects, like the impact of inhibitory nodes,[27] the effect of short-range sensory nodes (changing continuously λ_c and λ_b),[19] and retardation effects[18] were based on this analysis and the inspection of the activity-dependent branching ratio (BR) $b(M)$.[28]

In the Kinouchi–Copelli model, a *single* node j can excite node i with probability A_{ij}. Assuming a locally tree-like network, the probability that node i is excited at time $t+1$ is (more details in Appendix A)[2]

$$p_i^{t+1} = (1 - p_i^t)\left(\eta + (1-\eta)\left[1 - \prod_{j=1}^{N}(1 - p_j^t A_{ij})\right]\right), \tag{2}$$

which in the absence of external stimulus, $\eta = 0$, is to leading order,

$$p_i^{t+1} = \sum_{j=1}^{N} A_{ij} p_j^t, \tag{3}$$

satisfying linear stochasticity. In contrast, consider a locally tree network with N excitable nodes in which α *excited nodes* are required for exciting a destination node. Then, one can show (details in Appendix A) that in the leading order,

$$p_i^{t+1} = \frac{1}{\alpha!}\left(\sum_{j=1}^{N} A_{ij} p_j^t\right)^{\alpha}, \tag{4}$$

which does not satisfy linear stochasticity. In Sec. III, we generalize the Kinouchi–Copelli model to account for violations to linear stochasticity by postulating that the probability that a node gets excited is given by a sigmoid function of the input $\sum_{j=1}^{N} A_{ij} x_j^t$, which interpolates between a piecewise linear function and a threshold-type function that gives deterministic dynamics.

III. MODEL

Our model consists of N excitable nodes as described in Sec. II. The nodes are connected via a random directed graph where each pair of nodes is connected with probability q, resulting in an average node in- and out-degree $\langle k \rangle = q(N-1)$. The connection weights w_{ij} for the non-zero matrix entries are randomly and uniformly distributed in the interval $[0, 2\sigma]$, where σ is a tuning parameter. The leading control parameter is the largest eigenvalue of the network adjacency matrix A, which is $\lambda \approx \sigma q N$ in our case [see Eq. (1)].

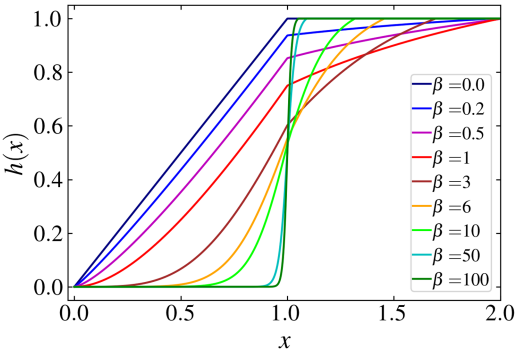

FIG. 1. Transfer function $h_\beta(x)$ in Eq. (5) interpolating between stochastic ($\beta = 0$) and deterministic ($\beta \to \infty$) spike dynamics.

The dynamics generalizes the Kinouchi–Copelli model presented in Sec. II, taking into account that some nodes are in the refractory period, i.e., a node cannot be excited immediately after being excited in the previous step. The probability that a node i spikes at time $t+1$ is given by

$$p_i^{t+1} = \delta_{x_i(t),0} h_\beta \left(\sum_{j=1}^{N} A_{ij} x_j^t \right), \tag{5}$$

where $\delta_{x_i(t),0}$ is unity if $x_i(t) = 0$ and zero otherwise, i.e., it is the effect of the refractory period of one time step. The transfer function h_β gives the probability that a node becomes active based on the total input $\sum_{j=1}^{N} A_{ij} x_j^t$. In the rest of the paper, we will use $h_\beta(x) = G(h_0(x,\beta))$, where $G(x)$ is x when $0 \le x \le 1$, 1 if $x > 1$, and 0 if $x < 0$, and $h_0(x,\beta)$ is

$$h_0(x,\beta) = \left(2 - \frac{2}{\pi}\tan^{-1}\beta\right) \frac{x^\beta}{x^\beta + 1} G(x). \tag{6}$$

The function $h_\beta(x)$, as shown in Fig. 1 for different values of β, interpolates between linear stochastic ($\beta = 0$ where the probability of spike increases linearly with the input potential[17,27]) and a step-like function of input that shows a deterministic dynamics ($\beta \to \infty$ where a node is excited only when the input potential exceeds a threshold, arbitrarily set to unity).

When $\beta \to 0$, it was shown that in the continuum limit for large network sizes, the model reduces to Wilson–Cowan equations[29] when both inhibitory and excitatory nodes (neurons) are present.[30]

In Sec. IV we show numerically and analytically that the addition of nonlinearity ($\beta > 0$) results in rich dynamics with discontinuous transitions and bistability.

IV. BIFURCATION DIAGRAM: DISCONTINUOUS TRANSITIONS AND BISTABILITY

In order to study the effect of nonlinearity on transition from subcritical to critical behavior, we simulated Eq. (5) numerically for various values of λ and β and monitored the fraction of excited nodes,

$$s^t = \frac{1}{N} \sum_{n=1}^{N} x_i^t. \tag{7}$$

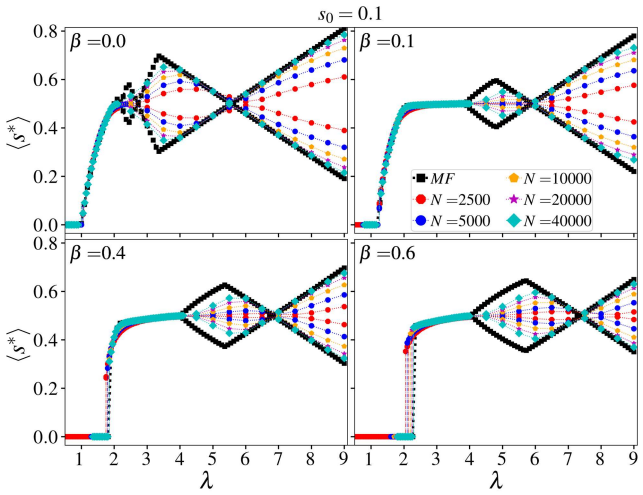

FIG. 2. Attractors of s^t, $\langle s^* \rangle$, as a function of λ for various values of β and N. The black bold squares are MF predictions obtained from the iterating map [Eq. (11)].

For simulations, we considered $N/10^3 = 2.5, 5, 10, 22$, and 40, with initial states chosen such that each node has $x_i = 1$ with probability 0.1 and $x_i = 0$ otherwise. 10^6 samples were generated for each λ, β, and N, over which ensemble averages were taken.

For a given realization of the dynamics, s^t either falls into the absorbing state $s = 0$ (subcritical regime), approaches a non-zero stationary state (supercritical regime), or oscillates between two non-zero values (oscillatory phase). Figure 2 shows the attractors s^* of s^t as a function of λ for various values of β and N. When $\beta = 0$ (top left), the system exhibits a second-order phase transition from the subcritical to the supercritical state at $\lambda = 1$ and a second transition to oscillations at $\lambda = 2$.[17] As we will demonstrate with a mean-field analysis, the behavior of the system in the oscillatory regime is highly dependent on the initial conditions, and the particular structure observed in Fig. 2 depends on the choice $s_0 \approx 0.1$. For positive values of β, the transition from the subcritical to the supercritical state becomes of first order, with the system transitioning from $s^* = 0$ to $s^* > 0$ in a discontinuous way at a value of $\lambda > 1$.

To understand these dynamics, we analyze the evolution of the system under the update equation (5) using a mean-field approach. Considering the expected value of s^{t+1}, we find using Eqs. (5) and (7)

$$\begin{aligned} \mathbb{E}\left[s^{t+1}\right] &= \frac{1}{N}\sum_{m=1}^{N} \mathbb{E}\left[x_m^{t+1}\right] \\ &= \frac{1}{N}\sum_{m=1}^{N} \mathbb{E}\left[\delta_{x_m^t,0} h_\beta \left(\sum_{n=1}^{N} A_{mn} x_n^t\right)\right]. \end{aligned} \tag{8}$$

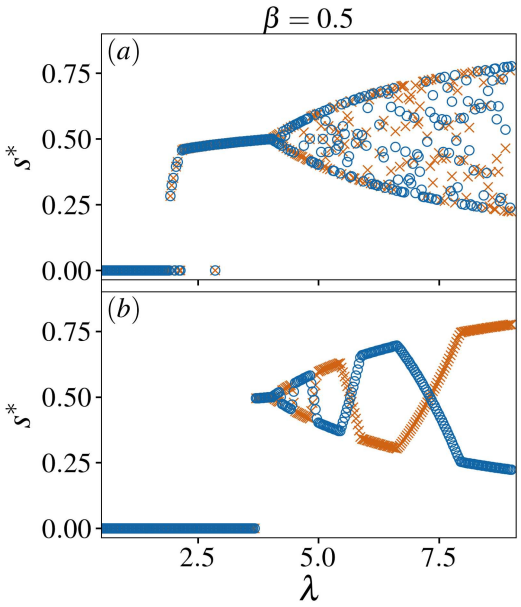

FIG. 3. Long-term values of even (circles) and odd (crosses) iterations of s^t obtained from the mean-field map [Eq. (11)] as a function of λ for $\beta = 0.5$. (a) The initial condition is random and uniformly chosen in [0, 1] for each λ. (b) The initial condition is 0.01 for each λ.

The sum over N in the previous equation can be interpreted as an average over nodes, which we will denote with $\langle\cdot\rangle$. Assuming independence of the random variables $\delta_{x_m^t,0}$ and $h_\beta\left(\sum_{n=1}^N A_{mn}x_n^t\right)$, we get

$$\mathbb{E}\left[s^{t+1}\right] = \left\langle\delta_{x_m^t,0}\right\rangle\left\langle h_\beta\left(\sum_{n=1}^N A_{mn}x_n^t\right)\right\rangle. \tag{9}$$

Now we use the fact that $\left\langle\delta_{x_m^t,0}\right\rangle = 1 - s^t$. Furthermore, for an Erdős–Rényi network with large mean degree, the distribution of the random variable $\sum_{m=1}^N A_{nm}x_m^t$ is narrow about its mean, λs^t, so we can approximate $\left\langle h_\beta\left(\sum_{j=1}^N A_{ij}x_j^t\right)\right\rangle \simeq h_\beta\left(\lambda s^t\right)$ to obtain

$$\mathbb{E}\left[s_{t+1}\right] \simeq (1 - s_t)h_\beta\left(\lambda s_t\right). \tag{10}$$

Focusing on the evolution of the expected value, we obtain the approximate one-dimensional map,

$$s^{t+1} \equiv f(s^t) = (1 - s_t)h_\beta\left(\lambda s_t\right). \tag{11}$$

Iteration of the map [Eq. (11)] with $s^0 = 0.1$ produces the black squares as shown in Fig. 2, which agree well with the simulations as N becomes large. Figure 3 shows the result of iterating the map [Eq. (11)] for $\beta = 0.5$ with two different initial conditions for each value of λ: for panel (a), s^0 is randomly and uniformly chosen in (0, 1), and in panel (b), s^0 is always 0.01.

To demonstrate how the map Eq. (11) can shed light into the dynamics of the system, including its dependence on the initial conditions as shown in Fig. 3, we plot the second iterate of the map, $f^{(2)}(s)$ vs s in Fig. 4 for $\beta = 0.5$ and $\lambda = 1$ (top panel), $\lambda = 2$ (middle panel), and $\lambda = 5$ (bottom panel). For $\lambda = 1$, the only fixed point is $s = 0$. As λ increases, a stable positive fixed point is created at $\lambda = \lambda_c$, such that for $\lambda = 2$, there are two stable fixed points. For $\lambda = 5$, there is a band of marginally stable period-2 orbits around $s = 0.5$. This band appears at $\lambda = 4$ and grows in size as λ is increased. Note that even for this high value of λ, the fixed point $s = 0$ remains stable, as can be seen in the inset that shows that the derivative $f'(0)$ is less than one (it is, in fact, 0). The inset also shows that although the fixed point $s = 0$ (the absorbing state) is stable, its basin of attraction is very small. With these observations, one can explain the qualitative features of Fig. 3 as follows. In panel (a) for $\lambda > 4$, initial conditions that fall inside the band of fixed points alternate between two values, producing the cloud of points that grows in size as the size of the band grows. For $\lambda_c < \lambda < 4$, almost all initial conditions fall within the basin of attraction of the positive stable fixed point, but a few get attracted to the still stable fixed point $s = 0$. For $\lambda < \lambda_c$, all initial conditions get attracted to the stable fixed point $s = 0$. In panel (b), the initial condition $s^0 = 0.01$ belongs to the basin of attraction of $s = 0$ up to approximately $\lambda \approx 3.7$. Beyond that, the orbit gets attracted to the stable fixed point first and to a period-2 orbit thereafter.

While some specific details about the bifurcation diagram depend on the shape of the transfer function h_β (such as the continuous band of marginally stable period-2 orbits), the general behavior of the system is as follows: for $\beta = 0$, there is a second-order phase transition from the subcritical to the supercritical regime, and a subsequent transition to an oscillatory regime. For $\beta > 0$, however, the transition is discontinuous and occurs at a value of λ larger than one. The absorbing state $s^* = 0$ remains stable, but its basin of attraction is extremely small. The phase diagram of the model is presented in Fig. 5.

V. HYSTERESIS AND FINITE SIZE EFFECTS

In Sec. IV, we found that for $\beta > 0$ the transition from the subcritical to the supercritical state is discontinuous. However, a mean-field analysis that assumed $N \to \infty$ revealed that the absorbing state $s^* = 0$ remains stable even for $\lambda > \lambda_c$. Therefore, it is important to understand how finite-size effects can drive the system away from the absorbing state. In this section, we address this by studying numerically and analytically the behavior of the system with initial conditions where only one node is excited, i.e., $s^0 = 1/N$. Note that in the thermodynamic limit, and using the mean field description derived above, this would yield $s^t = 0$ for $t > 0$ due to the linear stability of the absorbing state.

First, we study numerically the long-term behavior of the system under these initial conditions. For a given realization of the dynamics out of the oscillatory regime, the system either falls into the absorbing state $s^t \to s_1^* = 0$ or it reaches a steady state with $s^t \approx s_2^* > 0$. In Fig. 6(a), we show the probability distribution function (PDF) of s^* in terms of β obtained from 10^6 realizations of the dynamics. The PDF shows a bimodal structure, i.e., there are two peaks at $s_1^* = 0$ and $s_2^* > 0$. For small values of λ, there is only one peak at $s_1^* = 0$, showing that the system falls into the absorbing state with high probability. When λ is increased, the second peak s_2^* is born for the first time at a point that we denote by $\lambda_c^{(1)}(\beta)$ (see illustration in Fig. 6). As λ is increased further, the position of the first

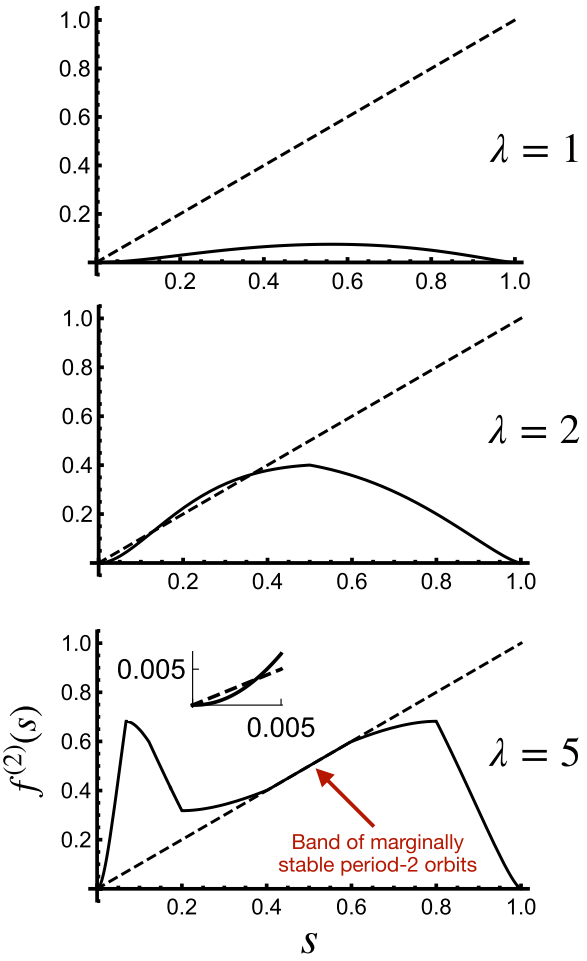

FIG. 4. Second iteration $f^{(2)}(s)$ of the mean field map [Eq. (11)] for $\lambda = 1$ (top), $\lambda = 2$ (middle), and $\lambda = 5$ (bottom). For small λ, the only fixed point is the absorbing state $s^* = 0$. For intermediate λ, a second stable fixed point emerges. For large λ, a band of marginally stable period-2 orbits is created, while the absorbing state is still stable but with a very small basin of attraction (inset).

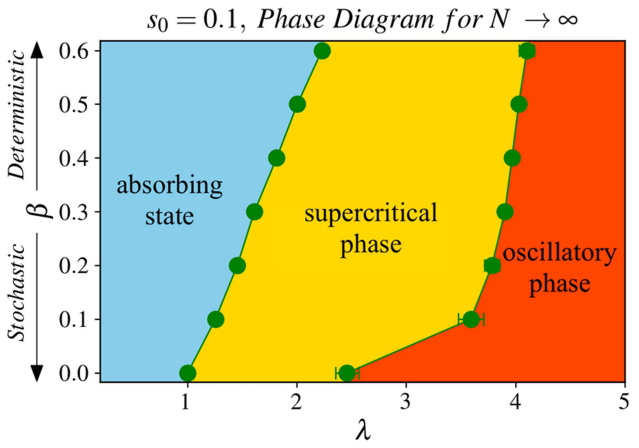

FIG. 5. The phase diagram of the model. Note that the supercritical and oscillatory phases coexist with the absorbing state, but the latter has an extremely small basin of attraction.

peak is fixed, while the second peak moves to the right, and at the same time the height of the first (second) peak decreases (increases), and eventually the first peak dies at a point that we call $\lambda_c^{(2)}(\beta)$. This reveals that the system exhibits a discontinuity at the point where the second peak is born $[\lambda_c^{(1)}(\beta)]$ using which we define a *gap parameter* as $\Delta(\beta) \equiv s_2^* - s_1^*$. As is shown in the inset of Fig. 6(a), $\Delta(\beta)$ saturates for large enough βs, and also $\lim_{\beta\to 0} \Delta = 0$, i.e., the gap closes at $\beta = 0$. The presence of two peaks with a gap in between is a signature of a *first-order transition*, while the zero gap in $\beta = 0$ suggests similarities with a *second-order transition* as is well-established in the literature.

As a standard approach for bimodal PDFs,[31] we divide the data at the valley point between s_1^* and s_2^* [with PDFs represented by $P_1(s^*)$ and $P_2(s^*)$, respectively] and average to find two $\langle s^* \rangle_i$, $i = 1, 2$ for two branches. The results are shown in Fig. 7 for various values of β and N. In these graphs, the upper branch [calculated from $P_2(s^*)$] is born for the first time at $(\lambda_c^{(1)}(\beta), \Delta(\beta))$ as explained above, and the lower branch [calculated from $P_1(s^*)$] dies at the point $[\lambda_c^{(2)}(\beta), 0]$. As λ increases further, the graph passes a bifurcation point $\lambda_b(\beta)$ beyond which the upper branch splits into (and oscillates between) two branches, the distance between which increases by increasing λ (first observed by Moosavi *et al.*[17]). From the behavior shown in Fig. 7, one observes hysteresis behavior, i.e., the loops that are extended from $\lambda_c^{(1)}$ to $\lambda_c^{(2)}$ between two branches. The survival of the lower branch is expected since the dynamics starts from one excited node, and there is a significant probability that activity dies out as we will show below. As β increases, the hysteresis effect magnifies and $\lambda_c^{(1,2)}$ grow with β and N, as is shown in Fig. 8(a) (similar results for $\lambda_c^{(2)}$ are not shown).

As discussed above, the coexistence of the two branches is caused by the fact that a single excited node can either cause excitations that become self-sustaining (leading to the branch $s_2^* > 0$) or fail to propagate its activity (leading to $s_1^* = 0$). Therefore, an important question is to determine when the excitation of a single node will lead to the absorbing state $s^* = 0$. We will approach this problem by examining the expected evolution of Eq. (5) when only one node is excited at time $t = 0$ and calculating the expected number of nodes that are excited at time $t = 1$, Ns_1. If $s_1 > s_0 = 1/N$, we expect that, on average, activity will grow and the absorbing state will not be reached. Assuming that node i is initially excited, we have

$$x_n^1 = \begin{cases} 1 & \text{with probability } h_\beta\left(\sum_{m=1}^N A_{nm} x_m^t\right),\ n \neq i \\ 0 & \text{otherwise.} \end{cases} \tag{12}$$

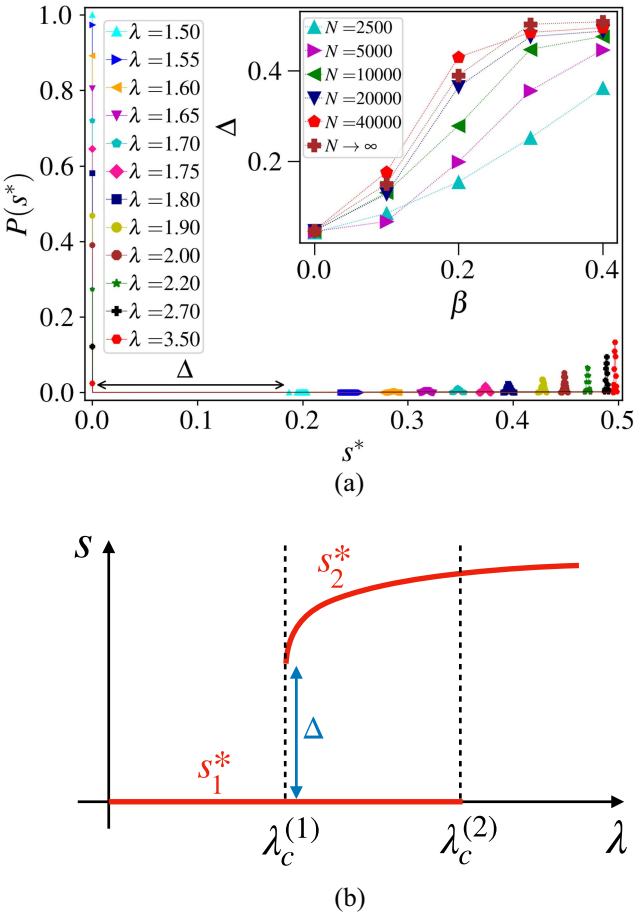

FIG. 6. (a) The distribution function $P(s^*)$ of s^* for the case $s^0 = 1/N$ shown for various values of λ and N for $\beta = 0.2$. The inset shows the gap $\Delta(\beta)$ as a function of β. (b) Schematic illustration of the quantities $\lambda_c^{(1)}(\beta)$, $\lambda_c^{(2}(\beta)$, and $\Delta(\beta)$.

The expected network activity $s_t \equiv \frac{1}{N}\sum_{n=1}^{N} x_n^t$ at $t = 1$ is given by

$$\mathbb{E}[s_1] = \frac{1}{N}\sum_{n=1}^{N}\mathbb{E}\left[x_n^1\right] = \frac{1}{N}\sum_{n\neq i}^{N} h_\beta\left(\sum_{m=1}^{N} A_{nm}x_m^0\right), \tag{13}$$

where $\mathbb{E}[s_t]$ is the ensemble average of s_t. Since $x_n^0 = \delta_{n,i}$, this simplifies to

$$\mathbb{E}[s_1] = \frac{1}{N}\sum_{n\neq i}^{N} h_\beta\left(A_{ni}\right). \tag{14}$$

The adjacency matrix is weighted, and we can write $A_{nm} = a_{nm}w_{nm}$, where a_{nm} is 1 (0) if nodes n, m are connected (not connected). We choose the weights w_{nm} randomly and independently from a uniform distribution in $[0, 2\sigma]$, where σ is chosen so that the largest eigenvalue of the matrix A is λ. (However, we note

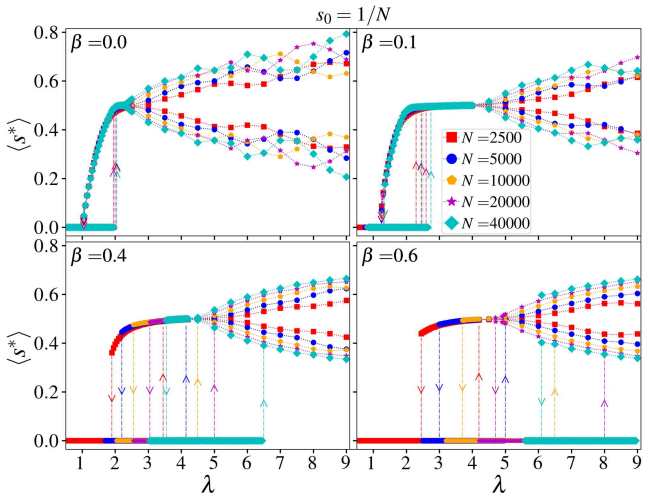

FIG. 7. Peaks $\langle s^* \rangle$ of the distribution $P(s^*)$ (see text) as a function of λ for various values of β and N for the case $s^0 = 1/N$. Hysteresis is identified by dashed lines with arrows.

that the following arguments work with more general weight distributions.) Since the network is Erdős–Rényi with mean degree $\langle k \rangle$, we can approximate $\langle k \rangle \sigma \approx \lambda$. Rewriting the right hand side of the previous equation as an average over nodes,

$$\mathbb{E}[s_1] = \frac{1}{N}\sum_{n\neq i}^{N} a_{ni}h_\beta\left(w_{ni}\right) = \langle a h_\beta\left(w\right)\rangle, \tag{15}$$

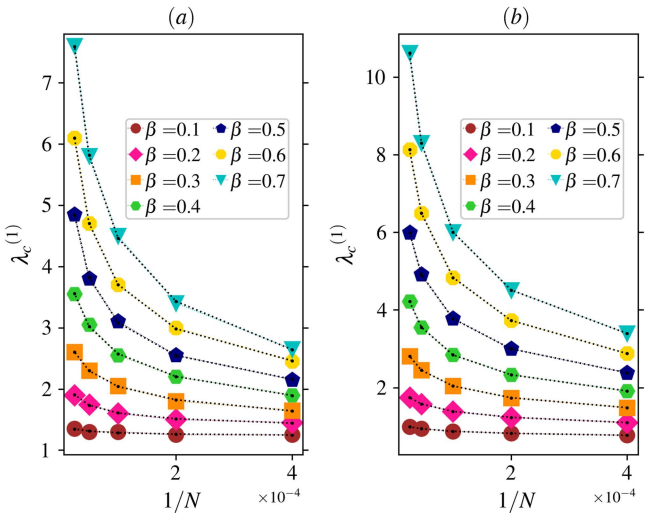

FIG. 8. (a) Values of $\lambda_c^{(1)}$ obtained numerically for various values of N and β. (b) Values of $\lambda_c^{(1)}$ obtained from Eq. (21) for the same values of N and β.

and using independence, we find

$$\mathbb{E}[s_1] = \langle a \rangle \langle h_\beta(w) \rangle = \frac{\langle k \rangle}{N} \langle h_\beta(w) \rangle. \tag{16}$$

Calculating the average over the uniform distribution of weights and using $s_0 = 1/N$, we obtain

$$\frac{\mathbb{E}[s_1]}{s_0} = \langle k \rangle \frac{\langle k \rangle}{2\lambda} \int_0^{2\lambda/\langle k \rangle} h_\beta(w)\, dw. \tag{17}$$

Changing variables, we find that the transition point separating the regimes where the single node ends in the absorbing or supercritical state is a solution to

$$\frac{\mathbb{E}[s_1]}{s_0} = 1 = \langle k \rangle \int_0^1 h_\beta \left(\frac{2u\lambda}{\langle k \rangle} \right) du. \tag{18}$$

Equation (18) gives a relation between the mean degree $\langle k \rangle$, the transfer function h_β, and the largest eigenvalue λ determining the effective boundary between the absorbing state and the supercritical state for finite networks. To demonstrate its validity, numerical results and the theoretical prediction from Eq. (18) are shown in Fig. 9 for (N, q) equal to $(5000, 0.01)$, $(500, 0.1)$, $(5000, 0.1)$, and $(500, 0.01)$. The red line shows the curve defined by Eq. (18) in the (β, λ) plane. The blue dots correspond to numerical simulations of the full system that end up in the absorbing state $s_1^* = 0$ and the clear dots to simulations that end up with positive activity s_2^*. The theory predicts well the boundary between the two behaviors. Note that the boundary depends on $\langle k \rangle$ and not on N, which is illustrated in Figs. 9(a) and 9(b) that have the same value of $\langle k \rangle$ but different N.

If $\mathbb{E}[s_1] < s_0$ (blue regions in Fig. 9), we expect that the activity will die out in a finite number of time steps (one can think of activity in this case as a subcritical branching process). The upper branch, characterized by a nonzero probability that activity becomes self-sustained, appears when $\mathbb{E}[s_1] > s_0$ (a supercritical branching process). Therefore, we identify $\lambda_c^{(1)}$ as the value of λ that solves Eq. (18). In the thermodynamic limit $N \to \infty$, one can expand the integrand in Eq. (18) to get an analytic approximation to $\lambda_c^{(1)}$. We use the following expansion for $\varepsilon \ll 1$:

$$h_\beta(\varepsilon) = 2 \left(1 - \frac{1}{\pi} \tan^{-1} \beta \right) \varepsilon^{1+\beta} + \text{higher orders of } \varepsilon, \tag{19}$$

so that Eq. (18) becomes in the limit $N \to \infty$ (using $\langle k \rangle = qN$),

$$1 = \frac{2^{2+\beta}}{2+\beta} \left(1 - \frac{1}{\pi} \tan^{-1} \beta \right) \left(\frac{\lambda^{1+\beta}}{q^\beta N^\beta} \right). \tag{20}$$

Therefore, the critical $\lambda_c^{(1)}$ is found to be

$$\lambda_c^{(1)} = \left(\frac{(2+\beta)\, q^\beta}{2^{2+\beta}(1 - \frac{1}{\pi} \tan^{-1} \beta)} \right)^{\frac{1}{1+\beta}} N^{\frac{\beta}{1+\beta}}. \tag{21}$$

This shows that when $N \to \infty$, $\lambda_c^{(1)}$ diverges for non-zero βs, so that for finite λ values, the system will always end in the absorbing state. In Fig. 8(b), we plot the theoretical prediction from Eq. (21). While the theoretical values do not agree exactly with the numerical observations shown in Fig. 8(a), the theory predicts well the qualitative features, including the dependence on β and N.

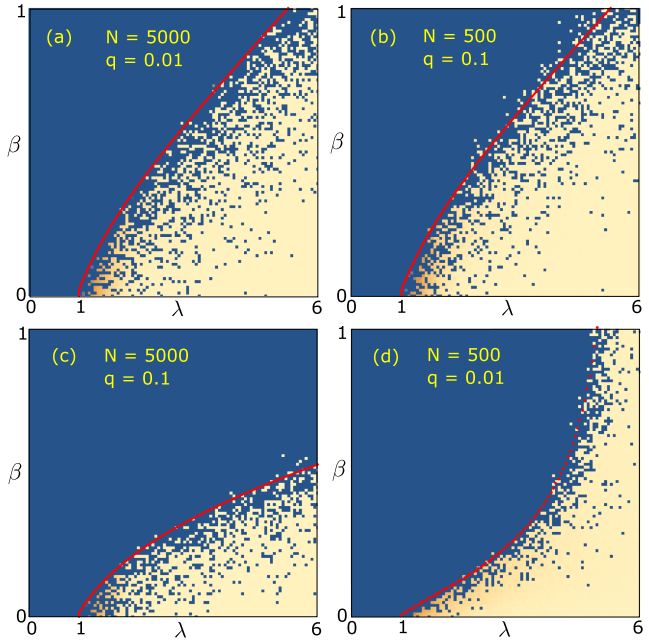

FIG. 9. Simulation and MF results for the phase diagram of the system for the case $s^0 = 1/N$ with the parameters equal to (a) $N = 5000$ and $q = 0.01$, (b) $N = 500$ and $q = 0.1$, (c) $N = 5000$ and $q = 0.1$, and (d) $N = 500$ and $q = 0.01$. The blue (clean) areas show systems that end up in the absorbing (supercritical) state. The red line shows the criterion given by the MF analysis, i.e., Eq. (18).

In Fig. 10, we show a numerically obtained phase diagram for the case $s^0 = 1/N$ for three values of N. As discussed above, in the thermodynamic limit, the dominant phase for all λ values and $\beta > 0$ is the absorbing state. However, Eq. (21) shows that for low values of β, the supercritical phase can persist for large values of N, in agreement with Fig. 10.

VI. DISCUSSION

We investigated a model for networks of an excitable system that interpolates between linear stochastic and threshold deterministic dynamics. We found that the introduction of nonlinearity in the transfer function for small input values (characterized in our model by positive values of the parameter β) results in bistability between the absorbing state $s^* = 0$ and a supercritical state with $s^* > 0$. For positive values of β, the supercritical state s^* appears at a value of the network eigenvalue $\lambda > 1$ and with a positive gap $\Delta = s^* > 0$, resulting in hysteretic behavior. In addition, for larger values of λ, an oscillatory phase appears as has been reported previously for similar models.[17] A mean-field analysis of the dynamics provides insights into the dynamics of the model and good quantitative agreement with numerical simulations, including its dependence on initial conditions, the linear stability and small basin of attraction of the absorbing state, and the particular nature of the oscillatory phase. The main insight obtained from the mean-field analysis is that any amount of nonlinearity creates bistability between the absorbing

state and the supercritical state, but the basin of attraction of the absorbing state is typically very small. The phase diagram for the system is shown in Fig. 5 in the limit $N \to \infty$.

We also studied the behavior of the model for large but finite networks. As a representative case of initial conditions consisting of a small number of excited nodes, we studied in detail the case of a single initially excited node. Using probabilistic arguments, we derived conditions on the parameters under which we expect such an initial condition to fall into the absorbing state. Using this condition, we were able to obtain an analytical formula for the value of λ below which the system is attracted to the absorbing state. From the theoretical analysis, we found that all initial conditions with $s^0 = 1/N$ fall into the absorbing state for large enough N, in agreement with our finding that the absorbing state is linearly stable in the mean-field analysis. However, our theoretical result shows how the behavior of a finite but large network differs from that of an idealized infinite network. For example, Fig. 5 shows that the effective phase diagram for $N = 40\,000$ can be very different from the $N \to \infty$ phase diagram, and Eq. (21) shows how, for small values of β, the difference can persist for very large values of N. The phase diagram for the system is shown in Fig. 10 for finite N.

Some features of our analysis depend on specific model choices. For example, the existence of the band of marginally stable period-2 orbits depends on the choice of the transfer function in Fig. 1. However, our main results, namely, that (i) the addition of nonlinearity to the transfer function in $(0, 1)$ causes the appearance of a positive branch $s^* > 0$ with a positive gap as illustrated in Fig. 6(b), (ii) that a mean-field analysis allows the study of the collective dynamics in the limit $N \to \infty$, and (iii) that a probabilistic analysis allows the analysis of the fate of initial conditions with a single excited node in large but finite networks, are independent of these choices. To see this, note that both the mean-field analysis leading to Eq. (11) and the probabilistic analysis leading to Eq. (18) do not depend on the particular transfer function used.

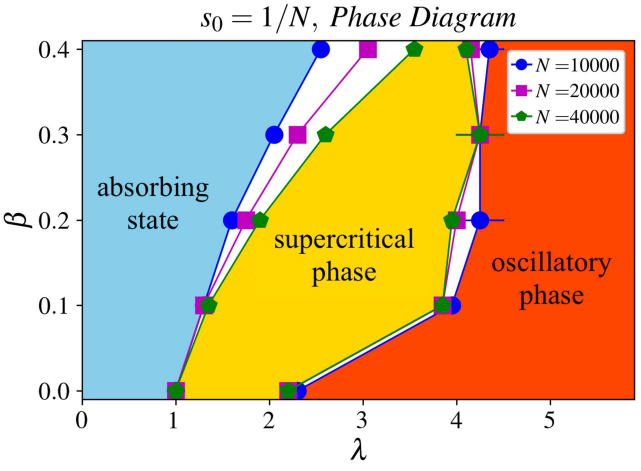

FIG. 10. Numerically obtained phase diagram for the case $s^0 = 1/N$ for three values of N.

In our model, the dynamics is stochastic for finite β and deterministic for $\beta \to \infty$. An interesting question is whether the addition of noise to the deterministic dynamics $\beta \to \infty$ might effectively be represented by a finite value of β. We leave this question for future research.

Our results show that even a small degree of nonlinearity (e.g., compare the curves $\beta = 0$ and $\beta = 0.2$ in Fig. 1) can have dramatic consequences for the dynamics of large networks of excitable units. Since it is often assumed that excitation between excitable units is non-cooperative, which is implemented with a piecewise linear transfer function, care should be taken when interpreting the results of models with such assumptions.

AUTHOR DECLARATIONS

Conflict of Interest

The authors have no conflicts to disclose.

Author Contributions

M. Rahimi-Majd: Data curation (equal); Formal analysis (equal); Visualization (equal). **J. G. Restrepo:** Methodology (equal); Validation (equal); Writing – original draft (equal). **M. N. Najafi:** Conceptualization (equal); Methodology (equal); Project administration (equal); Supervision (equal).

APPENDIX A: KINOUCHI–COPELLI (KC) MODEL AND GENERALIZATION

In this Appendix, we explain how the Kinouchi–Copelli (KC) model can be generalized to account for cooperative interactions.

Let us start with the KC model for a system with N excitable nodes and the variable $\{x_i\}_{i=1}^N$, which takes $m+1$ values $0, 1, \ldots, m$ in which 0 is the rest state and 1 is the excited state, and $x_i = 2, \ldots, m$ are the refractory states. If node $x_i(t) = 0$, it becomes excited in the next step $[x_i(t+1) = 1]$ by a neighboring excited node j with probability A_{ij} or independently by an external stimuli with probability η. The nodes in the refractory state evolve as $x_i(t+1) = x_i(t) + 1$ if $1 \le x_i(t) < m - 1$ and $x_i(t+1) = 0$ if $x_i(t) = m$. For $m = 1$, it is not hard to show[2] that (assuming a locally tree-like network)

$$p_i^{t+1} = (1 - p_i^t)\left(\eta + (1-\eta)\left[1 - \prod_j^N (1 - p_j^t A_{ij})\right]\right). \quad \text{(A1)}$$

Note that the first factor guarantees that the site i is in rest at time t. To understand the second factor, note that if $p_j^t A_{ij} = 0$ for all neighbors, then $p_i^{t+1} = (1 - p_i^t)\eta$ (which is due to external stimuli) and when $p_j^t A_{ij} = 1$ for at least one j, then $p_i^{t+1} = (1 - p_i^t)$, i.e., it turns on definitely if $p_i^t = 0$. Then, for testing the stability of the solution $p^* = 0$, one can expand the equation for small p_i^t's (to the first order) and in the limit of zero external stimuli, the following equation is obtained:

$$p_i^{t+1} = (1 - p_i^t)\eta + (1-\eta)\sum_j^N p_j^t A_{ij} \to \sum_j^N p_j^t A_{ij}, \quad \text{(A2)}$$

which admits the solution $p_i^t = \lambda^t u_i$, where u_i and λ are the eigenvector and (largest) eigenvalue of the A matrix. Equation (A1) holds for the case where at least one node can excite another node. Now let us consider the case where *two* excited nodes are necessary for exciting *one* node. Then this equation changes to

$$p_i^{t+1} = (1 - p_i^t)\left(\eta + (1-\eta)\left[1 - \prod_{j>k}^{N}(1 - p_j^t p_k^t A_{ij} A_{ik})\right]\right), \quad \text{(A3)}$$

which for small p limit and $\eta \to 0$ casts to

$$p_i^{t+1} = \sum_{j>k} p_j^t p_k^t A_{ij} A_{ik} = \frac{1}{2}\left[\left(\sum_{j}^{N} p_j^t A_{ij}\right)^2 - \sum_{j}^{N}\left(p_j^t A_{ij}\right)^2\right] \quad \text{(A4)}$$

for which the first term is the leading term (the first term contains $\sim N^2$ terms, while the second contains $\sim N$ terms). For a general case where α excited nodes are required for exciting, we obtain for large N

$$p_i^{t+1} \to \frac{1}{\alpha!}\left(\sum_{j=1}^{N} p_j^t A_{ij}\right)^{\alpha}, \quad \text{(A5)}$$

which is a generalized version of the KC model. Note that summing over all possible αs gives $\exp\left[\sum_j^N p_j^t A_{ij}\right] - 1$, which is a standard (exponential) dynamic function (a normalization factor is needed) used in a large class of excitable networks.

DATA AVAILABILITY

The data that support the findings of this study are available within the article.

REFERENCES

[1] O. Kinouchi and M. Copelli, "Optimal dynamical range of excitable networks at criticality," Nat. Phys. **2**, 348–351 (2006).
[2] D. B. Larremore, W. L. Shew, and J. G. Restrepo, "Predicting criticality and dynamic range in complex networks: Effects of topology," Phys. Rev. Lett. **106**, 058101 (2011).
[3] D. B. Larremore, M. Y. Carpenter, E. Ott, and J. G. Restrepo, "Statistical properties of avalanches in networks," Phys. Rev. E **85**, 066131 (2012).
[4] W. L. Shew, H. Yang, T. Petermann, R. Roy, and D. Plenz, "Neuronal avalanches imply maximum dynamic range in cortical networks at criticality," J. Neurosci. **29**, 15595–15600 (2009).
[5] K. Finlinson, W. L. Shew, D. B. Larremore, and J. G. Restrepo, "Optimal control of excitable systems near criticality," Phys. Rev. Res. **2**, 033450 (2020).
[6] M. S. Abe, "Functional advantages of Lévy walks emerging near a critical point," Proc. Natl. Acad. Sci. U.S.A. **117**, 24336–24344 (2020).
[7] W. P. Clawson, N. C. Wright, R. Wessel, and W. L. Shew, "Adaptation towards scale-free dynamics improves cortical stimulus discrimination at the cost of reduced detection," PLoS Comput. Biol. **13**, e1005574 (2017).
[8] S. H. Gautam, T. T. Hoang, K. McClanahan, S. K. Grady, and W. L. Shew, "Maximizing sensory dynamic range by tuning the cortical state to criticality," PLoS Comput. Biol. **11**, e1004576 (2015).
[9] J. M. Beggs and D. Plenz, "Neuronal avalanches in neocortical circuits," J. Neurosci. **23**, 11167–11177 (2003).
[10] T. Petermann, T. C. Thiagarajan, M. A. Lebedev, M. A. Nicolelis, D. R. Chialvo, and D. Plenz, "Spontaneous cortical activity in awake monkeys composed of neuronal avalanches," Proc. Natl. Acad. Sci. U.S.A. **106**, 15921–15926 (2009).
[11] W. Gerstner, W. M. Kistler, R. Naud, and L. Paninski, *Neuronal Dynamics: From Single Neurons to Networks and Models of Cognition* (Cambridge University Press, 2014).
[12] C. V. Stewart and D. Plenz, "Homeostasis of neuronal avalanches during postnatal cortex development in vitro," J. Neurosci. Methods **169**, 405–416 (2008).
[13] L. De Arcangelis, C. Perrone-Capano, and H. J. Herrmann, "Self-organized criticality model for brain plasticity," Phys. Rev. Lett. **96**, 028107 (2006).
[14] L. de Arcangelis and H. J. Herrmann, "Learning as a phenomenon occurring in a critical state," Proc. Natl. Acad. Sci. U.S.A. **107**, 3977–3981 (2010).
[15] J. C. Miller, "Percolation and epidemics in random clustered networks," Phys. Rev. E **80**, 020901 (2009).
[16] A. Allard, P.-A. Noël, L. J. Dubé, and B. Pourbohloul, "Heterogeneous bond percolation on multitype networks with an application to epidemic dynamics," Phys. Rev. E **79**, 036113 (2009).
[17] S. A. Moosavi, A. Montakhab, and A. Valizadeh, "Refractory period in network models of excitable nodes: Self-sustaining stable dynamics, extended scaling region and oscillatory behavior," Sci. Rep. **7**, 1–10 (2017).
[18] M. Najafi and M. Rahimi-Majd, "The effect of retardation in the random networks of excitable nodes, embeddable in the Euclidean space," Phys. Scr. **94**, 055208 (2019).
[19] M. Rahimi-Majd, M. Seifi, L. de Arcangelis, and M. Najafi, "Role of anaxonic local neurons in the crossover to continuously varying exponents for avalanche activity," Phys. Rev. E **103**, 042402 (2021).
[20] W. L. Shew and D. Plenz, "The functional benefits of criticality in the cortex," Neuroscientist **19**, 88–100 (2013).
[21] D. B. Larremore, W. L. Shew, E. Ott, and J. G. Restrepo, "Effects of network topology, transmission delays, and refractoriness on the response of coupled excitable systems to a stochastic stimulus," Chaos **21**, 025117 (2011).
[22] Z. Ma, G. G. Turrigiano, R. Wessel, and K. B. Hengen, "Cortical circuit dynamics are homeostatically tuned to criticality in vivo," Neuron **104**, 655–664 (2019).
[23] M. Najafi, "Bak–Tang–Wiesenfeld model in the finite range random link lattice," Phys. Lett. A **378**, 2008–2015 (2014).
[24] M. Najafi, S. Tizdast, and J. Cheraghalizadeh, "Some properties of sandpile models as prototype of self-organized critical systems," arXiv:2009.08160 (2020).
[25] M. Najafi and H. Dashti-Naserabadi, "Statistical investigation of avalanches of three-dimensional small-world networks and their boundary and bulk cross-sections," Phys. Rev. E **97**, 032108 (2018).
[26] D. J. Watts, "A simple model of global cascades on random networks," Proc. Natl. Acad. Sci. U.S.A. **99**, 5766–5771 (2002).
[27] D. B. Larremore, W. L. Shew, E. Ott, F. Sorrentino, and J. G. Restrepo, "Inhibition causes ceaseless dynamics in networks of excitable nodes," Phys. Rev. Lett. **112**, 138103 (2014).
[28] E. Martin, A. Shreim, and M. Paczuski, "Activity-dependent branching ratios in stocks, solar x-ray flux, and the Bak-Tang-wiesenfeld sandpile model," Phys. Rev. E **81**, 016109 (2010).
[29] H. R. Wilson and J. D. Cowan, "Excitatory and inhibitory interactions in localized populations of model neurons," Biophysical J. **12**, 1–24 (1972).
[30] M. Benayoun, J. D. Cowan, W. van Drongelen, and E. Wallace, "Avalanches in a stochastic model of spiking neurons," PLoS Comput. Biol. **6**, e1000846 (2010).
[31] T. Xue, X. Li, P. Grassberger, and L. Chen, "Swarming transitions in hierarchical societies," Phys. Rev. Res. **2**, 042017 (2020).